CrossMark

Heat of hydration prediction for blended cements

Natallia Shanahan[1] · Victor Tran[1] · A. Zayed[1]

Abstract Prediction and control of concrete temperature rise due to cement hydration is of great significance for mass concrete structures since large temperature gradients between the surface and the core of the structure can lead to cracking thus reducing durability of the structure. Cement replacement with supplementary cementitious materials (SCMs) is frequently used to reduce the concrete temperature rise. Several models have been proposed for predicting heat release of blended cements; however, none of them address incorporation of metakaolin into the mixture. Isothermal calorimetry measurements, based on statistical experimental design, were taken on pastes incorporating combinations of SCMs and chemical admixtures. The data were then used to develop equations to predict the total heat reduction with the incorporation of chemical admixtures and SCMs. Analysis of the calorimetry data indicated that chemical admixtures do not have a significant effect on heat evolution beyond 12 h. SCMs investigated in this study (fly ash, slag, silica fume and metakaolin), on the other hand, were found to have a significant effect at hydration ages of 12, 24, 48 and 72 h.

✉ Natallia Shanahan
  nkashalo@mail.usf.edu

[1] Department of Civil and Environmental Engineering, University of South Florida, 4202 E. Fowler Ave., Tampa, FL 33620, USA

Introduction

Considerable amounts of heat liberated during cement hydration lead to an increase in temperature which typically occurs several hours after concrete placement. Since thermal conductivity of concrete is low, large temperature gradients can develop between the surface exposed to ambient temperature conditions and the core of the structure. These temperature gradients are of particular concern for mass concrete structures, where thermal stresses can lead to early-age cracking. In Florida, due to the warmer climate, thermal gradients can lead to cracking even in structures which would not normally be considered mass concrete, such as concrete pavement [1]. Reduction in early-age thermal cracking risk is typically achieved by reducing the heat of hydration and, therefore, concrete temperature rise. The recommended strategies for reducing the amount of heat generated during cement hydration include the use of low-heat portland cements, blended cements and partial cement replacement with supplementary cementitious materials (SCMs) [2].

Prediction and control of concrete temperature rise due to cement hydration is of great significance for mass concrete structures since large temperature gradients between the surface and the core of the structure can lead to cracking thus reducing durability of the structure. A number of models have been proposed to predict heat evolution from cement hydration reactions [3–6].

However, it has been well established that incorporation of SCMs affects the heat evolution concrete and temperature development [7–9]. This effect depends not only on the total amount of cement replacement, but also on the type of SCM used. Both fly ash (FA) and blast furnace slag (SL) have low reactivity at early hydration ages, although slag is believed to be more reactive than fly ash [10].

Springer

Therefore, addition of both of these SCMs is expected to decrease the heat of hydration at early ages and concrete temperature rise [9, 11–14]. Nevertheless, Pane and Hansen [14] note that although both FA and SL at 25% cement replacement result in lower total heat evolution during early ages compared to the plain cement sample, the total heat generated by BSF samples appears to exceed that of the control mixture beyond 3 days.

Silica fume (SF) and metakaolin (MK) are generally believed to increase the heat of evolution. However, contradictory reports can be found in the literature regarding the effect of both of these materials on heat of hydration and temperature rise. Kadri and Duval [15] observed an increase in the total heat with SF addition up to 30% in the first 24 h. This increase was more pronounced at low w cm^{-1} ratios. On the contrary, Mostafa and Brown [16] reported a slight reduction in total heat during the first 24 h with 10, 20 and 30% SF addition. After this time, there was a slight increase in the total heat for the mixture containing 10% SF, while the others continued to exhibit total heats below that of the plain cement sample. Pane and Hansen [14] confirmed that the effect of SF is dependent on the w cm^{-1} ratio of the mixture.

Frias et al. [17] reported a slight increase in the heat of hydration with MK addition compared to OPC. Kadri et al. [18] recorded a more notable increase in heat of hydration and temperature rise with 10% MK. Ambroise et al. [19] and Bai and Wild [20] observed an increase in the maximum temperature rise during hydration with up to 20% MK addition, while Kim et al. [21] reported a slight decrease in the maximum adiabatic temperature with addition of 10% MK. Jiang et al. [22] found the effect of cement replacement with MK on heat evolution to be dosage-dependent. At 6% MK addition, the total heat was significantly increased compared to the OPC mixture up to approximately 48 h, while at 10 and 14% cement replacement, a decrease in the total heat was observed. Bai and Wild [20] reported that an increase in temperature rise with MK addition can be counteracted by incorporation equal amounts of pulverized-fuel ash (PFA). The idea of combining several mineral admixtures in order to reduce heat evolution and concrete temperature rise is attractive, especially in the case of MK, as its addition can improve early-age compressive strengths typically associated with cement replacement by SL or FA [23, 24].

Several models have been proposed for predicting heat release of blended cements. Most of these models have been developed for binary combinations of OPC and slag [25–29]. A model incorporating SF and superplasticizer has been proposed as well [30]. Wang et al. [31] proposed an equation for total heat release for mixtures incorporating both slag and fly ash. Schindler and Folliard [8] also proposed a model incorporating the effects of slag and fly ash,

which was later modified to incorporate silica fume as well [32]. Poole et al. [33] and Riding et al. [7] demonstrated that chemical admixtures can impact hydration as well and should be taken into account when modeling hydration processes. However, none of the models to date address the effect of MK on heat evolution. The only guidance regarding the heat of hydration (HOH) of MK comes from Gajda [34] who states that it can be approximated as "100–125% that of Portland cement". This, however, applies only to OPC/MK mixtures, and it is unclear how the total heat evolution of ternary or quaternary systems will be modified by the addition of MK with chemical admixtures.

Additionally, all of the above models consider the effects of each SCM and each chemical admixture on hydration to be additive. However, there are indications in the literature that there may be more complex interactions between SCMs and therefore possibly chemical admixtures. Han et al. [35] investigated the effect of cement replacement with slag and cement replacement with low-CaO fly ash (binary combinations of OPC and each SCM) on heat release. Although the authors did not model the heat release of these binary systems, they observed that the heat reduction was "not proportional to the dosage of mineral admixtures". Palou et al. [36] also observed in the OPC-SL-SF-MK systems that the total heat of hydration is not proportional to cement content reduction.

The absence of a predictive equation for heat evolution incorporating MK as well as the possibility of interactions between certain SCM or chemical admixture combinations served as a motivation for this study. The goal of the study was to assess the effect of commonly used SCMs and chemical admixtures as well as their potential interactions on cumulative heat evolution and to develop a set of equations that will allow engineers to estimate potential heat reduction resulting from the incorporation of different SCM and chemical admixtures combinations into a concrete mixture.

Experimental

Characterization of as-received materials

Type I/II commercial portland cement, four mineral admixtures (FA, SL, SF and MK) and three chemical admixtures, air-entraining admixture (AEA), water-reducing and retarding admixture (WRRA) and superplasticizer (SP), typically used in structural concrete in Florida, were selected for this study. X-ray fluorescence spectroscopy (XRF) was used to determine the chemical oxide composition of cement and mineral admixtures following ASTM C114 (Table 1).

Table 1 Oxide chemical composition of cement and mineral admixtures

Analyte	Cement/mass%	FA/mass%	SL/mass%	SF/mass%	MK/mass%
SiO_2	20.40	55.48	35.15	92.90	51.29
Al_2O_3	5.20	27.46	14.25	0.31	44.16
Fe_2O_3	3.20	6.70	0.48	0.10	0.49
CaO	63.10	0.99	41.45	0.78	<0.01
MgO	0.80	0.88	5.21	0.18	0.14
SO_3	3.60	0.05	1.86	<0.01	<0.01
Na_2O	0.10	0.29	0.22	0.10	0.26
K_2O	0.38	2.28	0.32	0.52	0.27
Total	100.10	99.93	99.83	99.63	99.22
Na_2O_{eq}	0.35	1.80	0.43	0.44	0.44
L.O.I (950 °C)	2.80	3.83	0.04	4.55	1.40

The mineralogical composition of cement and mineral admixtures was determined from X-ray diffraction (XRD) measurements in accordance with ASTM C1365 (Table 2). Prior to XRD measurements, cement was wet-ground in ethanol in a McCrone micronizing mill to a particle size between 1 and 10 μm. The wet grinding method was used to avoid the effect of temperature on gypsum and its possible phase transformation to hemihydrate or anhydrite. Since SCMs are known to have large amounts of amorphous content, ground mineral admixture samples were mixed with 10% titanium dioxide (TiO_2), which was used as an internal standard for quantification of the amorphous material. TiO_2 was obtained from the National Institute of Standards and Technology (NIST) as part of the Standard Reference Material (SRM) 674b set. Samples were mixed in the McCrone micronizing mill for 10 min with 5 mL of ethanol per every gram of sample as recommended by

Table 2 Mineralogical composition of cement and mineral admixtures

Cement			Mineral admixtures			
			FA	SL	SF	MK
C_3S	46.9	Mullite	16.1			1.0
C_2S	25.2	Hematite	1.6			
C_3A	9.6	Magnetite	1.1			
C_4AF	8.0	Quartz	9.0	1.4	1.9	0.3
Gypsum	2.8	Melilite		1.3		
Hemihydrate	1.8	Merwinite		0.1		
Anhydrite	0.5	CaO		0.1		
Calcite	2.0	Calcite		0.4		
Portlandite	2.5	Silicon carbide			2.0	
Quartz	0.8	Crystobalite			0.3	
		Illite				0.7
		Amorphous	72.2	96.7	95.8	98.0

ASTM C1365 in order to achieve homogeneous dispersion of the internal standard throughout the sample. The samples were then dried in an oven at 40 °C. XRD scans were collected using the Phillips X'Pert PW3040 Pro diffractometer equipped with the X'Celerator Scientific detector and a Cu-Kα x-ray source. Tension and current were set to 45 kV and 40 mA, respectively; 5 mm divergence and anti-scatter slits were used in the automatic mode. Phase quantification was performed using the Rietveld refinement functionality of the Panalytical HighScore Plus 3.0 software.

Particle size distribution (PSD) of the as-received materials was determined LA-950 laser scattering particle size analyzer manufactured by HORIBA Instruments using the dry method. Each measurement was taken in triplicate, and average values are reported in Table 3. As expected, metakaolin was finer than cement, while fly ash and slag had fineness values that were similar to that of cement. However, the particle size distribution for silica fume as well as its mean particle size (MPS) was significantly coarser than that of the other materials. This was unexpected, since over 95% of the silica fume particles are reported to be finer than 1 μm [37]. Since the silica fume used in this study is densified, it appears that the dry process of particle size analysis was unable to provide sufficient dispersion of the silica fume particles. This has been previously reported by Yajun and Cahyadi [38], who also observed agglomeration of densified silica fume when measured by laser diffraction. As suggested by [38], nitrogen adsorption with the Brunauer-Emmett-Teller (BET) method [39] was used to determine the surface area of silica fume, as well as the rest of the as-received materials, by nitrogen adsorption using an Autosorb-1 analyzer by Quantachrome Instruments. Samples were degassed under vacuum at 80°C immediately prior to analysis in order to remove any moisture or contaminants

Table 3 Particle size analysis of cement and mineral admixtures

Physical properties	Cement	FA	SL	SF	MK
$D_{10}/\mu m$	3.01	5.12	3.31	14.62	1.72
$D_{50}/\mu m$	13.02	9.94	10.86	50.52	5.48
$D_{90}/\mu m$	29.30	22.02	23.40	190.21	11.65
Mean particle size/μm	15.09	14.06	12.56	79.38	6.25
Multipoint BET surface area/m^2/kg	2140	2270	3700	21,410	14,970

Table 4 Experimental design addition levels

Design level	2	1	0	−1	−2
FA (fraction of total cementitious content)	0.40	0.30	0.20	0.10	0.00
SF (fraction of total cementitious content)	0.20	0.15	0.10	0.05	0.00
MK (fraction of total cementitious content)	0.20	0.15	0.10	0.05	0.00
SL (fraction of total cementitious content)	0.40	0.30	0.20	0.10	0.00
AEA (mL/100 kg cementitious)	46	34.5	23	11.5	0
WRRA (mL/100 kg cementitious)	400	300	200	100	0
SP (mL/100 kg cementitious)	200	150	100	50	0

from the sample surface. BET fineness values are included in Table 3, which shows that fineness of silica fume is significantly higher than what was indicated by the particle size analysis. Since the BET method is based on the physical adsorption of nitrogen gas molecules on the sample surface, it is not affected by agglomeration [38].

Factorial design

Factorial design was used to evaluate the effect of the selected SCMs and chemical admixtures on heat evolution. Factorial designs are commonly used in screening experiments to identify significant factors (mineral and chemical admixtures in this study) using the smallest number of experiments [40]. In concrete research, factorial designs have been previously used for mix design optimization [41–48]. The advantage of factorial designs is not only that they allow to reduce the number of experiments compared to "one factor at a time" approach, but they are also able to evaluate potential factor interactions.

Seven admixtures (factors) were identified for this study: Class F FA, SL, SF, MK, AEA, WRRA and SP. Coded values for each factor were used in the experimental design, which were calculated using the following general equation [40]:

$$\text{Coded value} = \frac{\left(\text{actual value} - \frac{(\alpha_{-1} + \alpha_1)}{2}\right)}{\frac{\alpha_1 - \alpha_{-1}}{2}} \quad (1)$$

Therefore, individual coded values for each variable were calculated as follows:

$$\text{FA}_{\text{coded}} = \text{SL}_{\text{coded}} = \frac{\text{actual value} - 0.20}{0.10} \quad (2)$$

$$\text{SF}_{\text{coded}} = \text{MK}_{\text{coded}} = \frac{\text{actual value} - 0.10}{0.05} \quad (3)$$

$$\text{AEA}_{\text{coded}} = \frac{\text{actual value} - 23}{11.5} \quad (4)$$

$$\text{WRRA}_{\text{coded}} = \frac{\text{actual value} - 200}{100} \quad (5)$$

$$\text{SP}_{\text{coded}} = \frac{\text{actual value} - 100}{50} \quad (6)$$

The dosages of each chemical and mineral admixture corresponding to each coded design value are listed in Table 4. A constant w cm^{-1} ratio of 0.485 was maintained for all the mixtures.

The use of coded variables is preferable in the initial analysis over actual (natural) values. Since the levels of each factor can differ greatly from each other, converting natural values to coded values allows the relative effect of each factor to be evaluated [40]. Additionally, the use of coded variables ensures that the root-mean-square error (RMSE) is the same for all the variables.

At first, a fractional factorial design was performed (design matrix is listed in Table 5). Fractional factorial designs are commonly used in screening experiments to identify significant factors using the smallest number of

experiments [40]. In concrete research, factorial designs have been previously used for mix design optimization [41–47]. The fractional factorial design was a resolution III design, which means that the effect of each factor could not be separated from the effect of two-factor interactions.

In order to improve the resolution, axial points and a center point were added to create central composite design (CCD) with $\alpha = 2$, where α is the distance from the center point for each factor. A 2D graphical illustration of CCD is presented in Fig. 1. Both experimental designs were created using JMP software from SAS. One run was performed for each mixture, except for the center point, where two runs were performed to assess the error associated with experimental results. CCD was a resolution IV design, in which main effects were not compounded with any two-factor interactions, but the two-factor interactions were compounded with each other. Additionally, since the CCD used five levels of each factor, it can be used to assess whether or not the response changed linearly with changing factor level. The design matrix for axial points is presented in Table 6.

Heat flow measurements were taken following external mixing protocol, Method B of ASTM C1702. All measurements were taken at an isothermal temperature of 23 °C. Pastes were mixed with an IKA WERKE mixer for a total of 7 min following the procedure described in [49]. WRRA was added to the mixing water. After combining water and cementitious materials, the paste was mixed for 1 min prior to the addition of AEA, after which it was mixed for an additional 2 min. The mixture was then rested for 2 min. After the rest period, SP was added to the

mixture, and the sample was mixed for an additional 2 min at 1200 rpm rather than 2000 rpm as reported by Muller et al. [49]. Upon completion of mixing, samples were immediately placed into the iCal-8000 Calmetrix isothermal calorimeter.

The cumulative heat values at 12, 24, 48 and 72 h were extracted from the collected data for each mixture. Since only one cement was used in this study, reduction in the
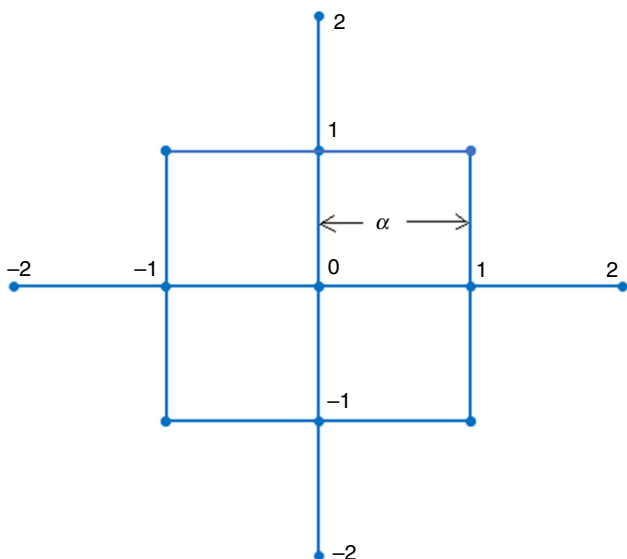
Table 5 Fractional factorial design matrix

Mix #	FA	SF	MK	SL	AEA	WRRA	SP
1	1	−1	−1	−1	−1	1	1
2	−1	−1	1	−1	1	1	−1
3	1	1	−1	−1	1	1	−1
4	−1	1	−1	−1	1	−1	1
5	−1	1	1	1	1	−1	−1
6	−1	−1	−1	−1	−1	−1	−1
7	1	−1	1	−1	1	−1	1
8	1	1	1	−1	−1	−1	−1
9	1	−1	−1	1	1	−1	−1
10	−1	−1	−1	1	1	1	1
11	−1	1	−1	1	−1	1	−1
12	1	1	−1	1	−1	−1	1
13	1	1	1	1	1	1	1
14	−1	−1	1	1	−1	−1	1
15	1	−1	1	1	−1	1	−1
16	−1	1	1	−1	−1	1	1

Fig. 1 Two-dimensional central composite design (CCD) representation

Table 6 Additional axial points design matrix

Mix #	FA	SF	MK	SL	AEA	WRRA	SP
17	2	0	0	0	0	0	0
18	−2	0	0	0	0	0	0
19	0	2	0	0	0	0	0
20	0	−2	0	0	0	0	0
21	0	0	2	0	0	0	0
22	0	0	−2	0	0	0	0
23	0	0	0	2	0	0	0
24	0	0	0	−2	0	0	0
25	0	0	0	0	2	0	0
26	0	0	0	0	−2	0	0
27	0	0	0	0	0	2	0
28	0	0	0	0	0	−2	0
29	0	0	0	0	0	0	2
30	0	0	0	0	0	0	−2
31	0	0	0	0	0	0	0
32	0	0	0	0	0	0	0

Table 7 Admixture addition rates for validation mixtures

Mix#	FA (fraction of total cementitious content)	SF	MK	SL	AEA	WRRA	SP
		(mL/100 kg cementitious)					
1	0.10	0.15	0.05	0.30	11.5	100	150
2	0.10	0.05	0.05	0.30	34.5	100	50
3	0.30	0.15	0.15	0.10	11.5	300	150
4	0.20	0.10	0.10	0.20	0	200	0
5	0.20	0.10	0.10	0.20	23	0	0
6	0.20	0.10	0.10	0.20	0	0	100
7	0.20	0.10	0.00	0.20	0	0	0
8	0.20	0.10	0.10	0.20	0	0	0
9	0.20	0.00	0.10	0.20	0	0	0
10	0.20	0.00	0.10	0.00	0	0	0
11	0.40	0.00	0.10	0.00	0	0	0
12	0.40	0.00	0.20	0.00	0	0	0
13	0.20	0.00	0.10	0.00	0	0	0
14	0.40	0.00	0.10	0.00	0	0	0
15	0.40	0.00	0.20	0.00	0	0	0
16	0.00	0.00	0.10	0.20	0	0	0
17	0.00	0.00	0.10	0.40	0	0	0
18	0.20	0.20	0.00	0.00	0	0	0
19	0.20	0.00	0.00	0.20	0	0	0
20	0.20	0.00	0.00	0.40	0	0	0
21	0.00	0.00	0.10	0.30	0	0	0
22	0.00	0.00	0.20	0.30	0	0	0
23	0.30	0.20	0.00	0.00	0	0	0
24	0.21	0.08	0.00	0.00	0	0	0
25	0.21	0.08	0.00	0.00	0	0	0
26	0.21	0.08	0.00	0.00	0	0	0
27	0.21	0.00	0.10	0.00	0	0	0
28	0.21	0.00	0.10	0.00	0	0	0
29	0.21	0.00	0.00	0.30	0	0	0
30	0.21	0.00	0.00	0.30	0	0	0
31	0.21	0.00	0.00	0.30	0	0	0
32	0.00	0.00	0.00	0.00	23	200	100
33	0.00	0.00	0.00	0.00	0	0	100
34	0.00	0.00	0.00	0.00	0	0	200
35	0.00	0.00	0.00	0.00	46	300	

total heat compared to the plain cement–water paste ($\Delta Q/Q_{OPC}$ between cumulative heat of the plain OPC-water mixture, Q_{OPC}, and the mixture modified by addition of SCM and/or chemical admixtures) was selected as a response variable rather than the total heat. Several studies demonstrated that the total heat evolution depends on cement fineness and mineral composition [3, 4, 50]. Therefore, it is expected that equations that model total heat reduction with SCM incorporation compared to the plain cement mixture would be more useful than those modeling the total heat based only on one OPC composition.

$\Delta Q/Q_{OPC}$ values calculated for each mixture were analyzed with JMP software to identify significant factors. A significance level of 95% was used in this study. In addition to the 32 mixtures that were used to generate the models, 35 additional mixtures were prepared for validation of these models. Admixture addition rates and their corresponding coded levels for the validation mixtures are listed in Tables 7 and 8, respectively.

Table 8 Validation mixtures coded levels for each factor

Mix #	FA	SF	MK	SL	AEA	WRRA	SP
1	−1	1	−1	1	−1	−1	1
2	−1	−1	−1	1	1	−1	−1
3	1	1	1	−1	−1	1	1
4	0	0	0	0	−2	0	−2
5	0	0	0	0	0	−2	−2
6	0	0	0	0	−2	−2	0
7	0	0	−2	0	−2	−2	−2
8	0	0	0	0	−2	−2	−2
9	0	−2	0	0	−2	−2	−2
10	0	−2	0	−2	−2	−2	−2
11	2	−2	0	−2	−2	−2	−2
12	2	−2	2	−2	−2	−2	−2
13	0	−2	0	−2	−2	−2	−2
14	2	−2	0	−2	−2	−2	−2
15	2	−2	2	−2	−2	−2	−2
16	−2	−2	0	0	−2	−2	−2
17	−2	−2	0	2	−2	−2	−2
18	0	2	−2	−2	−2	−2	−2
19	0	−2	−2	0	−2	−2	−2
20	0	−2	−2	2	−2	−2	−2
21	−2	−2	0	1	−2	−2	−2
22	−2	−2	2	1	−2	−2	−2
23	1	2	−2	−2	−2	−2	−2
24	0.1	−0.4	−2	−2	−2	−2	−2
25	0.1	−0.4	−2	−2	−2	−2	−2
26	0.1	−0.4	−2	−2	−2	−2	−2
27	0.1	−2	0	−2	−2	−2	−2
28	0.1	−2	0	−2	−2	−2	−2
29	0.1	−2	−2	1	−2	−2	−2
30	0.1	−2	−2	1	−2	−2	−2
31	0.1	−2	−2	1	−2	−2	−2
32	−2	−2	−2	−2	0	0	0
33	−2	−2	−2	−2	−2	−2	0
34	−2	−2	−2	−2	−2	−2	2
35	−2	−2	−2	−2	2	1	−2

Results and discussion

Model development

Based on the fractional factorial design, only FA and SL were identified as significant factors at 12 and 24 h. SF had a p value of 0.0502 at 24 h, so its significance was very close to 95%. All three of these factors had p values below

0.05 at 48 and 72 h. However, each of these individual factors was aliased with a number of factor combinations. Additionally, coefficients of determination (R^2 values) for the linear models varied from 0.72 to 0.83 depending on the hydration age, indicating that the fit could possibly be improved by addition of factor interactions or quadratic terms.

Addition of axial points and a center point increased the resolution of the design so that individual factors were no longer aliased with factor combinations and allowed quadratic effects to be evaluated as well. Statistical analysis showed that significant factors and factor combinations varied depending on the age of paste (Tables 9, 10).

Response surface methodology with least squares fitting was used to obtain coefficients (listed in Estimates columns of Tables 9, 10) for the significant factors and factor interactions. R^2 values for the models, at each hydration age, were significantly improved compared to those obtained from linear models based on the fractional factorial design.

The analysis was first performed using coded variables (Table 9). Since the modeled response was the reduction in total heat with addition of different admixtures, positive coefficients in Table 9 indicate that increase in those factors will result in a further decrease in the total heat. Negative coefficients, on the other hand, signify an increase in total heat with an increase in the factor level.

While significant factors at 12 h included both mineral and chemical admixtures, the contribution of chemical admixtures was determined to be insignificant after this age. The lack of significant effect of chemical admixtures on heat evolution after 12 h has been previously reported by Medina et al. [51]. At all ages, the largest reduction in the total heat was achieved by increasing FA and SL content. At 12 and 24 h, their coefficients were approximately the same, while at 48 and 72 h the coefficient for SL began to decrease. This decrease in the slag coefficient may possibly indicate that at these ages the hydration reaction of slag starts to contribute to the total heat evolution, therefore lowering the total heat reduction compared to the plain OPC mixture.

It is of interest that the statistical analysis identified SL^2 as a significant factor. The nonlinear effect of slag on the total heat is in line with the results reported by Han et al. [27, 35], who also observed a nonlinear reduction in heat with increasing cement replacement by SL. As for the other SCMs, their effect on the total heat evolution was linear.

Same factors and factor interactions, namely FA, SL, SF, MK, SL^2 and the interaction of FA and SL, were

Table 9 Parameter estimates of the statistical models based on coded values

	12 h/$R^2 = 0.96$		24 h/$R^2 = 0.93$		48 h/$R^2 = 0.93$		72 h/$R^2 = 0.92$	
	Estimate	Prob. $> |t|$	Estimate	Prob. $> |t|$	Estimate	Prob. $> |t|$	Estimate	Prob. $> |t|$
β_0 Intercept	0.407	0.000	0.421	0.000	0.396	0.000	0.376	0.000
β_1 FA	0.117	0.000	0.109	0.000	0.105	0.000	0.104	0.000
β_2 SL	0.114	0.000	0.106	0.000	0.089	0.000	0.083	0.000
β_3 SF	0.052	0.000	0.056	0.000	0.055	0.000	0.055	0.000
β_4 MK	0.037	0.000	0.050	0.000	0.044	0.000	0.043	0.000
β_5 SL^2	0.023	0.003	0.018	0.041	0.017	0.042	0.017	0.035
β_6 FA $\times$ SL	0.027	0.008	0.027	0.031	0.024	0.039	0.024	0.039
B_7 MK $\times$ SL	0.031	0.004	–	–	–	–	–	–
β_8 WRRA	0.020	0.015	–	–	–	–	–	–
β_9 AEA	−0.020	0.015	–	–	–	–	–	–
β_{10} SF $\times$ MK	0.024	0.017	–	–	–	–	–	–

Table 10 Parameter estimates of the statistical models based on natural values

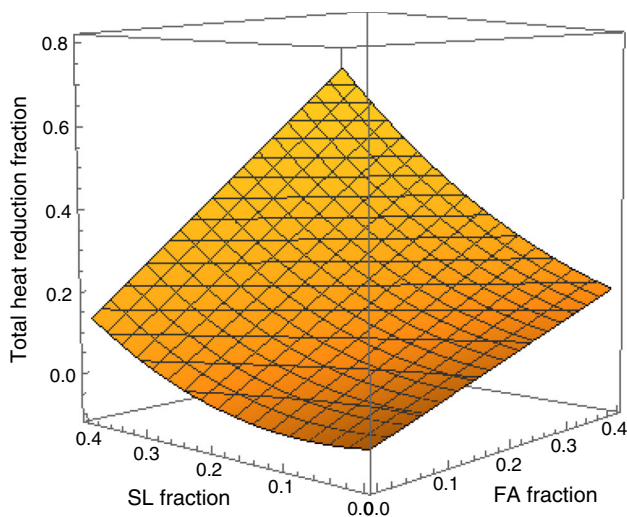|	12 h/$R^2 = 0.97$		24 h/$R^2 = 0.93$		48 h/$R^2 = 0.93$		72 h/$R^2 = 0.92$	
	Estimate	Prob. $> |t|$	Estimate	Prob. $> |t|$	Estimate	Prob. $> |t|$	Estimate	Prob. $> |t|$
β_0 Intercept	−0.231	0.000	−0.226	0.000	−0.191	0.000	−0.196	0.000
β_1 FA	1.166	0.000	1.095	0.000	1.053	0.000	1.045	0.000
β_2 SL	1.135	0.000	1.061	0.000	0.888	0.000	0.827	0.000
β_3 SF	1.047	0.000	1.130	0.000	1.103	0.000	1.109	0.000
β_4 MK	0.730	0.000	1.002	0.000	0.887	0.000	0.863	0.000
β_5 (SL-0.2)^2	2.299	0.002	1.846	0.041	1.712	0.035	1.758	0.000
β_6 (FA-0.2) $\times$ (SL-0.2)	2.734	0.005	2.683	0.031	2.385	0.039	2.358	0.001
B_7 (MK-0.1) $\times$ (SL-0.2)	6.140	0.002	–	–	–	–	–	–
β_8 WRRA	0.0002	0.009	–	–	–	–	–	–
β_9 AEA	−0.002	0.010	–	–	–	–	–	–
β_{10} (SF-0.1) $\times$ (MK-0.1)	9.750	0.011	–	–	–	–	–	–
β_{11} (FA-0.2) $\times$ (AEA-23)	−0.016	0.043	–	–	–	–	–	–

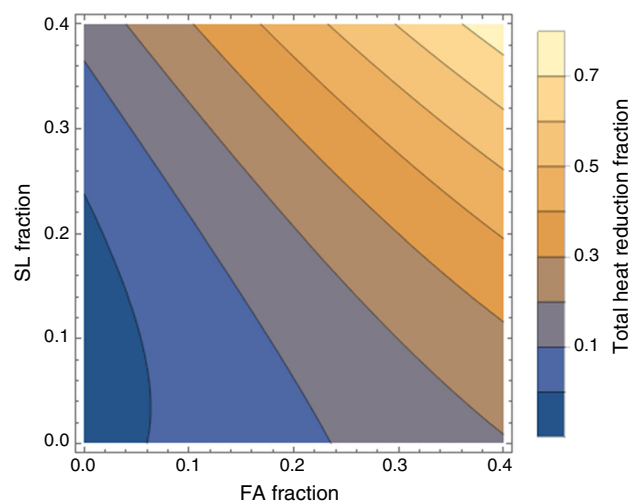**Fig. 2** Response surface plot for the change in FA and SL content using Eq. 8

Fig. 3 Contour plot of the total heat reduction with the change in FA and SL content
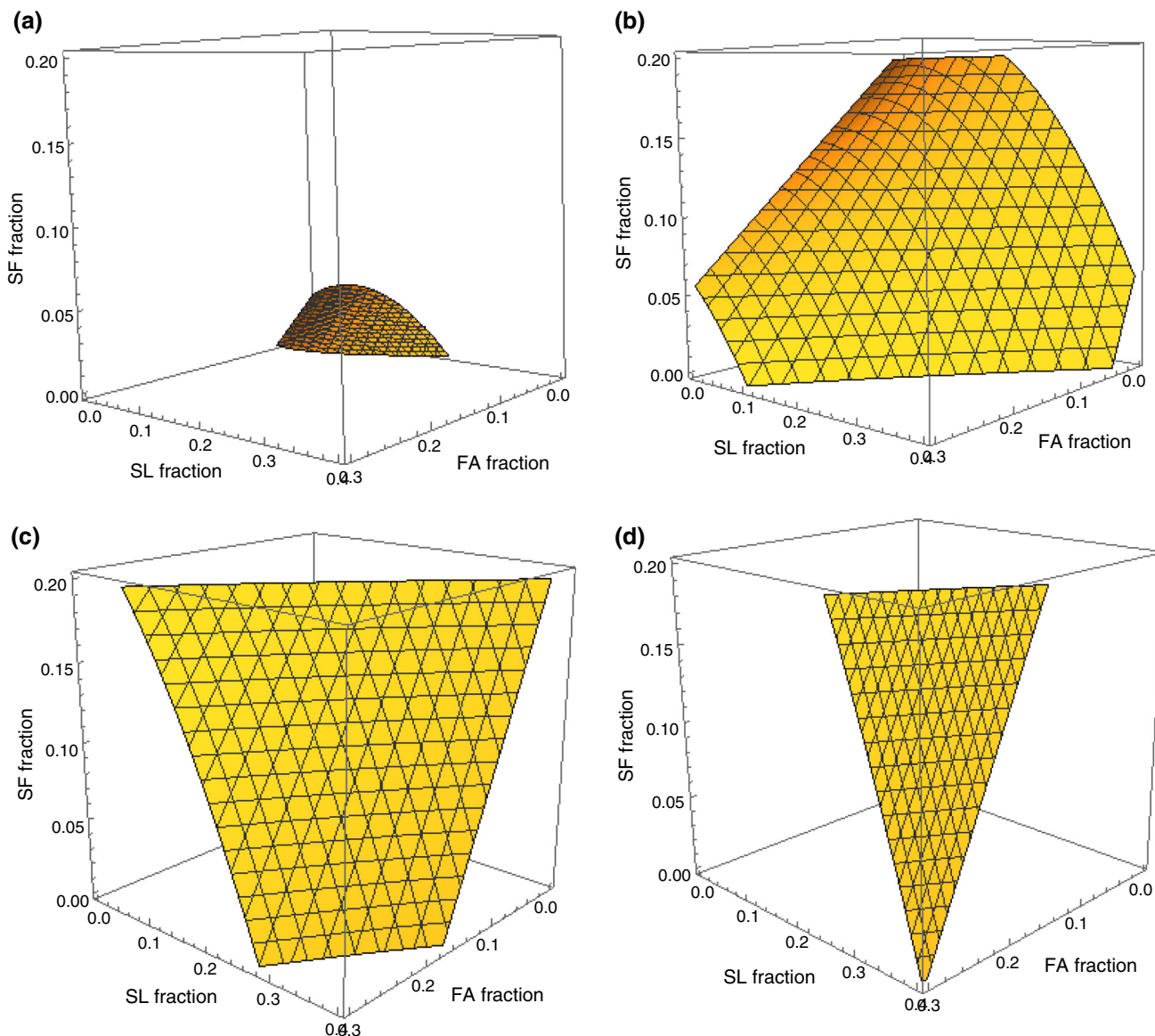
Fig. 4 Contour plot for the change in FA, SL and SF content using Eq. 8. **a** No change in cumulative heat evolved compared to the plain OPC-water mixture, **b** 20% cumulative heat reduction, **c** 40% cumulative heat reduction, **d** 60% cumulative heat reduction

identified as significant at 24, 48 and 72 h. Since the model coefficients were similar at these ages, a combined model for predicting total heat reduction at 24, 48 or 72 h was created as well:

$$\Delta Q/Q_{\mathrm{OPC}} \text{ coded} = 0.398 + 0.106 \cdot C_{\mathrm{FA}} + 0.092 \cdot C_{\mathrm{SL}}$$
$$+ 0.056 \cdot C_{\mathrm{SF}} + 0.046 \cdot C_{\mathrm{MK}}$$
$$+ 0.018 \cdot C_{\mathrm{SL}}^2 + 0.025 \cdot C_{\mathrm{FA}} \cdot C_{\mathrm{SL}} \tag{7}$$

where C_i is the ith coded level of each factor. It should be noted that the significance of all the coefficients in the combined model was 99% or greater.

Although the use coded variable is very helpful for statistical analysis, an equation based on natural values of each factor is more convenient practically. In addition to the coded variables, the analysis was also carried out based on the natural variables (Tables 5, 7). Again, a combined equation for the 24, 48 and 72 h total heat reduction was calculated as well:

$$\Delta Q/Q_{\mathrm{OPC}} = -0.034 + 0.569 \cdot P_{\mathrm{FA}} - 0.279 \cdot P_{\mathrm{SL}}$$
$$+ 1.114 \cdot P_{\mathrm{SF}} + 0.917 \cdot P_{\mathrm{MK}} \tag{8}$$
$$+ 1.772 \cdot P_{\mathrm{SL}}^2 + 2.475 \cdot P_{\mathrm{FA}} \cdot P_{\mathrm{SL}}$$

where P_i is the ith fraction of the total cementitious content for each factor.
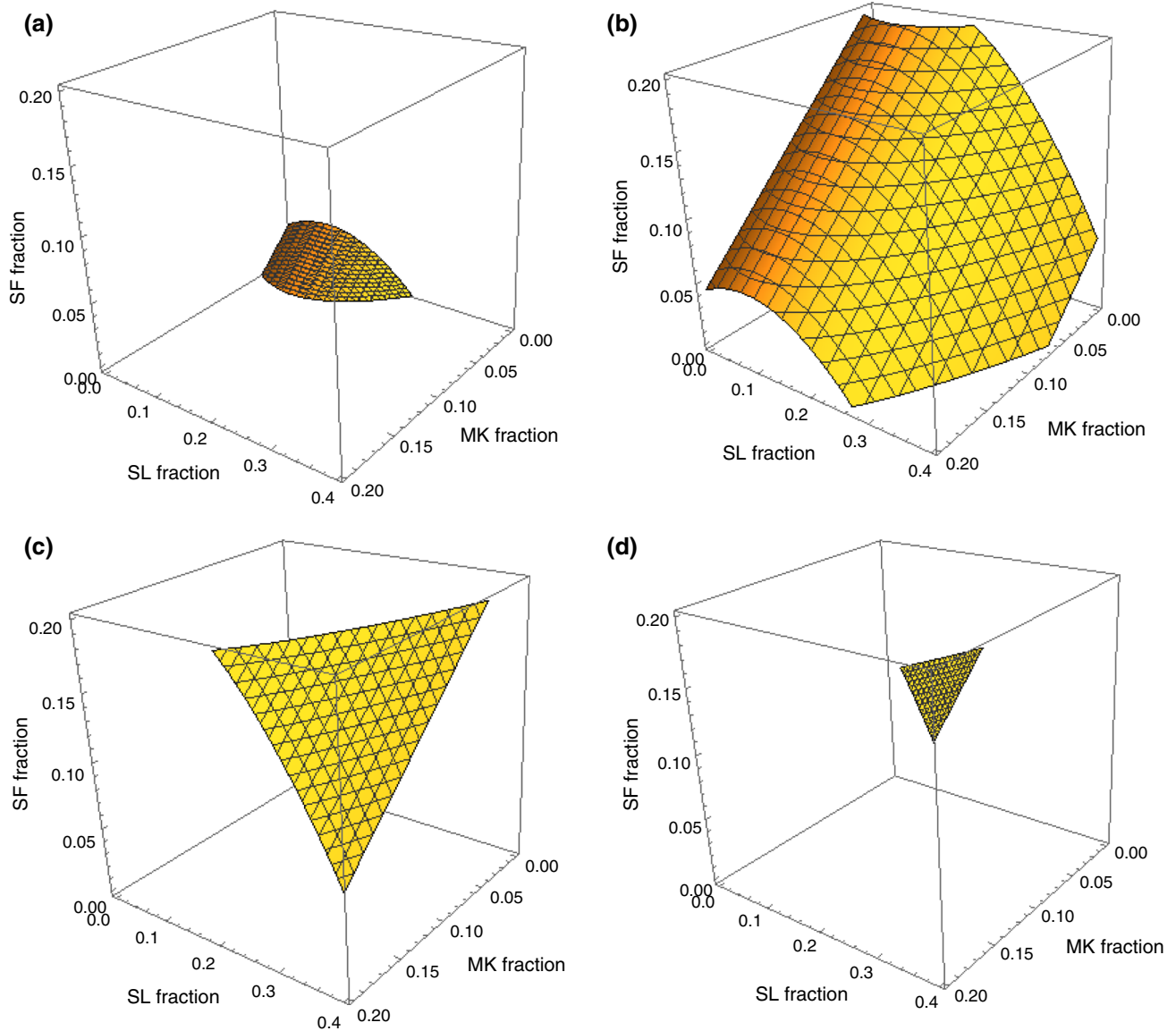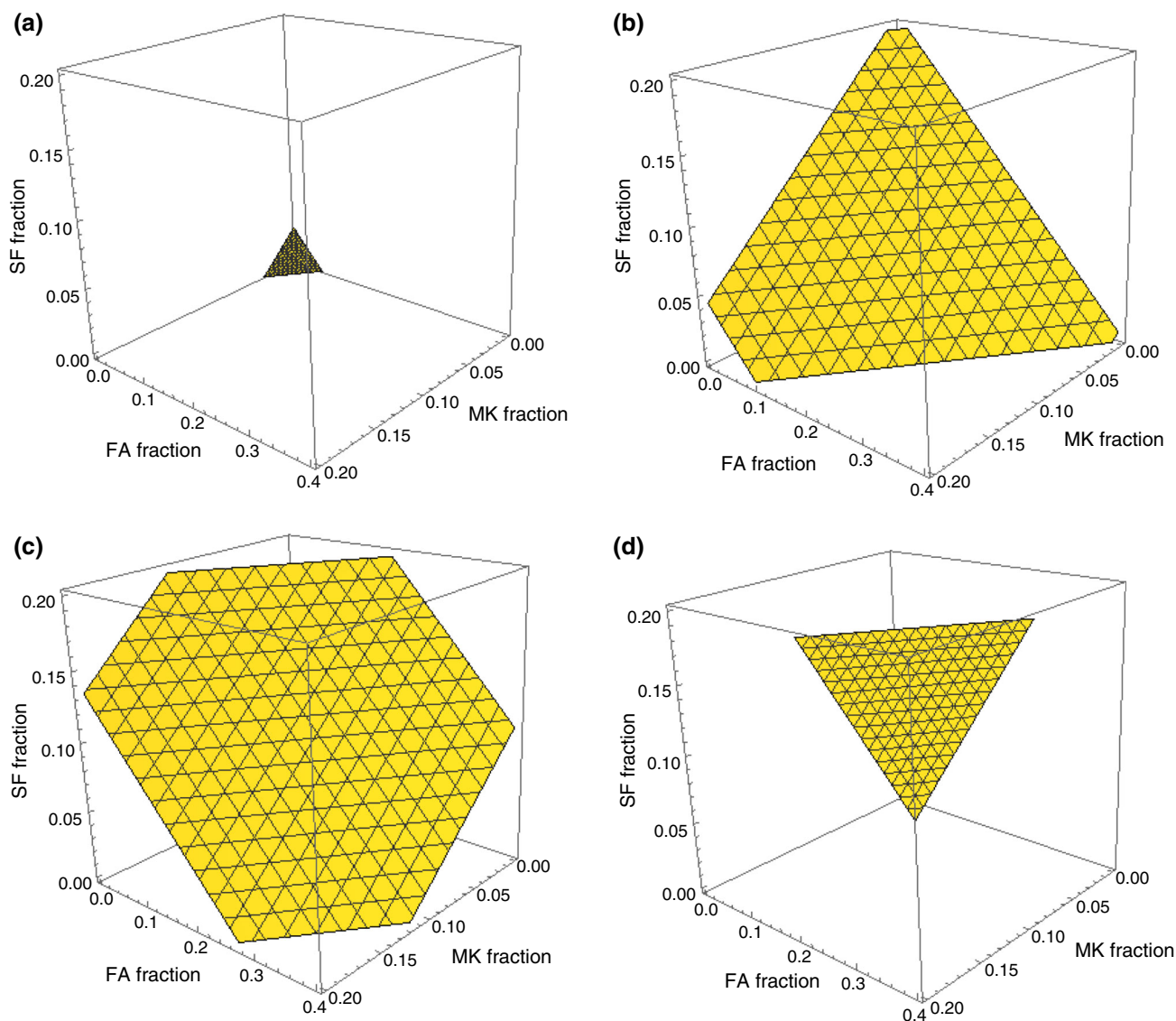
Fig. 5 Contour plot of the total heat reduction with the change in MK, SL and SF content using Eq. 8. **a** No change in cumulative heat evolved compared to the plain OPC-water mixture, **b** 20% cumulative heat reduction, **c** 40% cumulative heat reduction, **d** 50% cumulative heat reduction

Figures 2 and 3 show the relationship between the SL and FA content of the mixture and the total heat reduction. These figures clearly illustrate the nonlinear effect of SL on heat reduction. It is interesting to note that at small cement replacement levels, below 3% for FA and below 22% for SL, there is no reduction in cumulative heat.

Since it is not possible to generate a response surface plot for an equation with more than three variables,

Figs. 4–6 present three-dimensional contour plots for combinations of 3 SCMs resulting in a specified cumulative heat reduction. These figures illustrate that there are multiple SCM combinations that can produce the required reduction in heat evolution. Therefore, a lower hydration heat need not be the only consideration when selecting supplementary cementitious materials for cement replacement, and other concrete fresh and hardened properties can

Fig. 6 Contour plot of the total heat reduction with the change in MK, FA and SF content using Eq. 8. **a** No change in cumulative heat evolved compared to the plain OPC-water mixture, **b** 20% cumulative heat reduction, **c** 30% cumulative heat reduction, **d** 50% cumulative heat reduction

be taken into account in order to select the optimum SCM combination.

It is interesting to note that Fig. 4a illustrates that there are certain FA-SL-SF combinations that will not result in cumulative heat reduction at 24, 48 or 72 h. Essentially, the same plots are generated for the FA-SL-MK combinations, since the coefficients for MK and SF in Eq. 8 are very similar. Figures 5a and 6a also show regions of 0% heat reduction with addition of small amounts of SCMs.

Model validation

The model presented in Eq. 8 was validated by comparing heat reduction measured experimentally against the predicted values. The majority of the values lie within the 95% confidence interval (Fig. 7). Additionally, the data are evenly distributed around the line of fit, which indicates that there is no consistent bias in the model. Identical plot was obtained for Eq. 7 as this equation can be converted to Eq. 8 by substituting Eqs. 2 and 3 for the appropriated coded variables.
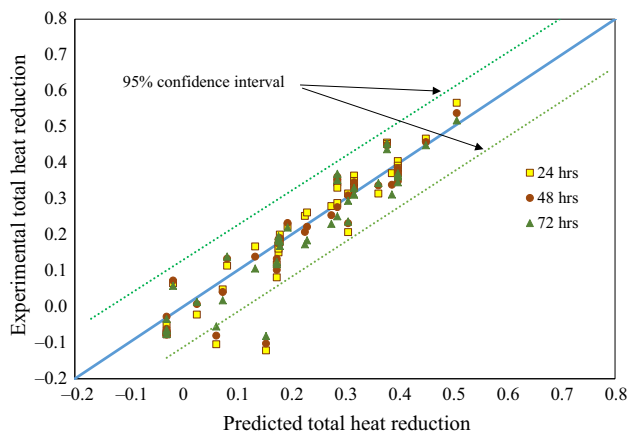
Fig. 7 Measured versus predicted total heat reduction calculated using Eq. 5.8

Conclusions

Statistical analysis of isothermal calorimetry data indicated that chemical admixtures do not have a significant effect on heat evolution beyond the hydration age of 12 h. SCMs investigated in this study (FA, SL, SF and MK), on the other hand, were found to have a significant effect at hydration ages of 12, 24, 48 and 72 h. While the effect of FA, SF and MK on the total heat reduction with increasing cement replacement appeared to be linear, the effect of SL was quadratic. The models proposed in this study were successful in predicting the total heat reduction with incorporation of chemical admixtures and SCMs compared to a plain OPC mixture. Since the proposed models predict the fraction of cumulative heat reduction compared to a plain OPC-water mixture, only one isothermal calorimetry measurement needs to be carried out. These models will allow practitioners to estimate heat reduction with the use of different SCM/chemical admixture combinations while avoiding multiple experimental testing.

References

1. Zayed A, Riding KA, Ferraro C, Bien-Aime AJ, Shanahan N, Buidens D, et al. Long-life slab replacement concrete. Tampa: University of South Florida; 2015.
2. ACI Committee 207. ACI 207.2R-07 report on thermal and volume change effects on cracking of mass concrete. Farmington Hills, MI: American Concrete Institute; 2007.
3. Poole T. Predicting seven-day heat of hydration of hydraulic cement from standard test properties. J ASTM Int. 2009;6:1–10.
4. Sedaghat A, Shanahan N, Zayed A. Predicting one-day, three-day, and seven-day heat of hydration of portland cement. J Mater Civ Eng. 2015;27:4014257.
5. Kishi T, Maekawa K. Multi-component model for hydration heat of Portland cement. Concr Libr JSCE. 1996;28:97–115.
6. Swaddiwudhipong S, Chen D, Zhang MH. Simulation of the exothermic hydration process of Portland cement. Adv Cem Res. 2002;14:61–9.
7. Riding KA, Poole JLJ, Folliard KJ, Juenger MCGG, Schindler AK. Modeling hydration of cementitious systems. ACI Mater J. 2012;109:225–34.
8. Schindler AK, Folliard KJ. Heat of hydration models for cementitious materials. ACI Mater J. 2005;102:24–33.
9. Bentz DP. A review of early-age properties of cement-based materials. Cem Concr Res. 2008;38:196–204.
10. Lothenbach B, Scrivener K, Hooton RD. Supplementary cementitious materials. Cem Concr Res. 2011;41:1244–56.
11. Neville AM. Properties of concrete. 4th ed. Harlow: Pearson Education Limited; 2006.
12. Mehta PK, Monteiro PJM. Concrete: microstructure, properties and materials. 3rd ed. New York: McGraw-Hill; 2006.
13. Osborne GJ. Durability of Portland blast-furnace slag cement concrete. Cem Concr Compos. 1999;21:11–21.
14. Pane I, Hansen W. Investigation of blended cement hydration by isothermal calorimetry and thermal analysis. Cem Concr Res. 2005;35:1155–64.
15. Kadri E-H, Duval R. Hydration heat kinetics of concrete with silica fume. Constr Build Mater. 2009;23:3388–92.
16. Mostafa NY, Brown PW. Heat of hydration of high reactive pozzolans in blended cements: isothermal conduction calorimetry. Thermochim Acta. 2005;435:162–7.
17. Frías M, De Rojas MIS, Cabrera J, Rojas MS de, Cabrera J. The effect that the pozzolanic reaction of metakaolin has on the heat evolution in metakaolin-cement mortars. Cem Concr Res. 2000 [cited 2013 Oct 2];30:209–16. http://cat.inist.fr/?aModele=afficheN&cpsidt=1338278.
18. Kadri E-H, Kenai S, Ezziane K, Siddique R, De Schutter G. Influence of metakaolin and silica fume on the heat of hydration and compressive strength development of mortar. Appl Clay Sci. 2011;53:704–8.
19. Ambroise J, Maximilien S, Pera J. Properties of metakaolin blended cements. Adv Cem Based Mater. 1994;1:161–8.
20. Bai J, Wild S. Investigation of the temperature change and heat evolution of mortar incorporating PFA and metakaolin. Cem Concr Compos. 2002;24:201–9.
21. Kim H-S, Lee S-H, Moon H-Y. Strength properties and durability aspects of high strength concrete using Korean metakaolin. Constr Build Mater. 2007;21:1229–37.
22. Jiang G, Rong Z, Sun W. Effects of metakaolin on mechanical properties, pore structure and hydration heat of mortars at 0.17 w/b ratio. Constr Build Mater. 2015;93:564–72.
23. Li Z, Ding Z. Property improvement of Portland cement by incorporating with metakaolin and slag. Cem Concr Res. 2003;33:579–84.
24. Khatib JM, Hibbert JJ. Selected engineering properties of concrete incorporating slag and metakaolin. Constr Build Mater. 2005;19:460–72.
25. Meinhard K, Lackner R. Multi-phase hydration model for prediction of hydration-heat release of blended cements. Cem Concr Res. 2008;38:794–802.
26. De Schutter G, Taerwe L. General hydration model for portland cement and blast furnace slag cement. Cem Concr Res. 1995;25:593–604.

27. Han F, Zhang Z, Wang D, Yan P. Hydration kinetics of composite binder containing slag at different temperatures. J Therm Anal Calorim. 2015;121:815–27.

28. Kolani B, Buffo-Lacarrière L, Sellier A, Escadeillas G, Boutillon L, Linger L. Hydration of slag-blended cements. Cem Concr Compos. 2012;34:1009–18.

29. Luan Y, Ishida T, Nawa T, Sagawa T. Enhanced model and simulation of hydration process of blast furnace slag in blended cement. J Adv Concr Technol. 2012;10:1–13.

30. Swaddiwudhipong S, Wu H, Zhang MH. Numerical simulation of temperature rise of highstrength concrete incorporating silica fume and superplasticiser. Adv Cem Res. 2003;15:161–9.

31. Wang XY, Cho HK, Lee HS. Prediction of temperature distribution in concrete incorporating fly ash or slag using a hydration model. Compos Part B Eng. 2011;42:27–40.

32. Folliard KJ, Juenger M, Schindler A, Riding KA, Poole JL, Kallivokas L, et al. Prediction model for concrete behavior—final report. Austin: Center for Transportation Research, the University of Texas at Austin; 2008.

33. Poole JJL, Riding KAK, Juenger MCG, Folliard KJ, Schindler AK. Effect of chemical admixtures on apparent activation energy of cementitious systems. J Mater Civ Eng. 2011;23:1654–62.

34. Gajda J. Mass concrete for buildings and bridges. Skokie: Portland Cement Association; 2007.

35. Han F, Liu R, Wang D, Yan P. Characteristics of the hydration heat evolution of composite binder at different hydrating temperature. Thermochim Acta. 2014;586:52–7.

36. Palou MT, Kuzielová E, Novotný R, Šoukal F, Žemlička M. Blended cements consisting of Portland cement–slag–silica fume–metakaolin system. J Therm Anal Calorim. 2016;125:1025–34.

37. Siddique R, Khan MI. Supplementary cementing materials. Berlin, Germany: Springer; 2011 [cited 2013 Sep 30]. http://www.springerlink.com/index/10.1007/978-3-642-17866-5.

38. Yajun J, Cahyadi JH. Effects of densified silica fume on microstructure and compressive strength of blended cement pastes. Cem Concr Res. 2003 [cited 2014 Feb 16];33:1543–8. http://linkinghub.elsevier.com/retrieve/pii/S0008884603001005.

39. Brunauer S, Emmett PH, Teller E. Adsorption of gases in multimolecular layers. J Am Chem Soc. 1938;60:309–19. http://pubs.acs.org/doi/abs/10.1021/ja01269a023.

40. Montgomery DC. Design and analysis of experiments. 6th ed. Hoboken: Wiley; 2005.

41. Sonebi M, Svermova L, Bartos PJM. Factorial design of cement slurries containing limestone powder for self-consolidating slurry-infiltrated fiber concrete. ACI Mater J. 2005;101:136–45.

42. Ghezal A, Khayat KH. Optimizing self-consolidating concrete with limestone filler by using statistical factorial design methods. ACI Mater J. 2002;99:264–72.

43. Khayat KH, Ghezal A, Hadriche MS. Factorial design models for proportioning self- consolidating concrete. Mater Struct. 1999;32:679–86.

44. Soudki K, El-Salakawy EF, Elkum N. Full factorial optimization of concrete mix design for hot climates. J Mater Civ Eng. 2001;13:427–33.

45. Patel R, Hossain K, Shehata M. Development of statistical models for mixture design of high-volume fly ash self-consolidating concrete. ACI Mater J. 2004;101:294–302.

46. Ferrara L, Park Y-D, Shah SP. A method for mix-design of fiber-reinforced self-compacting concrete. Cem Concr Res. 2007;37:957–71.

47. Srinivasan CB, Narasimhan NL, Ilango SV. Development of rapid-set high-strength cement using statistical experimental design. Cem Concr Res. 2003;33:1287–92.

48. Sonebi M. Factorial design modelling of mix proportion parameters of underwater composite cement grouts. Cem Concr Res. 2001;31:1553–60.

49. Muller ACA, Scrivener KL, Gajewicz AM, McDonald PJ. Use of bench-top NMR to measure the density, composition and desorption isotherm of C–S–H in cement paste. Microporous Mesoporous Mater. 2013;178:99–103.

50. Verbeck G, Foster C. Long-time study of cement performance in concrete: the heats of hydration of the cements. Proc Am Soc Test Mater Phila: PA; 1950. p. 1235–62.

51. Medina C, Sáez del Bosque IF, Asensio E, Frías M, Sánchez de Rojas MI. New additions for eco-efficient cement design. Impact on calorimetric behaviour and comparison of test methods. Mater Struct. 2016;49:4595–607.